International Journal of Heat and Mass Transfer 52 (2009) 952–961

Contents lists available at ScienceDirect

International Journal of Heat and Mass Transfer

journal homepage: www.elsevier.com/locate/ijhmt

Capillary-assisted flow and evaporation inside circumferential rectangular micro groove

Z.Z. Xia *, G.Z. Yang, R.Z. Wang

Institute of Refrigeration and Cryogenics, Shanghai Jiao Tong University, Shanghai 200240, PR China

ARTICLE INFO

Article history:
Received 24 July 2007
Received in revised form 16 February 2008
Available online 13 September 2008

Keywords:
Capillary-assisted evaporation
Micro groove
Rectangular cross section
Extended meniscus

ABSTRACT

To introduce capillary-assisted evaporation from micro-size fields to normal-size fields, an inclined circumferential micro groove with rectangular cross sections is investigated analytically and a systematic mathematical model is developed. The model is composed of five sub-models: a natural convection model, a liquid axial flow model, a heat transfer model in and below the intrinsic meniscus, an evaporation thin film region model and an adsorbed region model. In this model, for the extended meniscuses formed at groove cross sections, both the intrinsic meniscus and evaporation thin film region are considered when calculating heat absorbing. Through solving the model, the influences of dynamic contact angle on the heat absorbing in the intrinsic meniscus and evaporation thin film region are investigated. Moreover, the factors affecting the whole-groove equivalent heat transfer coefficient have been investigated.

1. Introduction

Capillary-assisted evaporation is a prevailing heat transfer method inside micro heat pipes which are widely used to cool down the micro or small-size equipments with high heat flux. Benefit from the ultra thin liquid film in the extended meniscus, capillary-assisted evaporation can achieve a very high local heat flux and heat transfer coefficient. For most previous researches [1–5], triangular grooves were focused on for two reasons: one is easy groove machining; the other is continuous heat flux at the groove bottom surface. Compared to triangular grooves, rectangular grooves have more liquid flow section area and, thus, smaller viscous friction force [6–9]. Accompany the liquid axial flow, the curvatures of the intrinsic meniscuses increase gradually and the dynamic contact angles minish. According to the literature [9], for rectangular grooves, "dead zone" will appear, followed by "corner flow", behind the groove axial location where the dynamic contact angle equals the minimum contact angle under the condition of non-zero liquid flow velocity and heat flux there. The occurrence of "corner flow" will harm the groove's ability to support super high heat flux. However, in normal equipments, we usually do not need so much heat flux and, by proper designing the groove's axial distance, "corner flow" can be avoided possibly. Given the assumption that the groove is liquid-full at liquid entry and the same minimum contact angles, a rectangular groove can supply larger driving force for liquid flow, and then support a larger axial flow rate than a triangular groove.

This work is motivated by introducing such kind of high efficient evaporation from micro-size fields to normal-size fields. The most outstanding advantage of capillary-assisted evaporation is that it does not need any assistant equipment to carry out liquid film distribution. Therefore, the evaporator can be designed to be very simple and compact which can reduce the cost and equipment size. For normal-size application, the micro grooves are usually machined on the outside surface of horizontal heat transfer tubes. When working, the bottom outside surfaces of heat transfer tubes are immersed in liquid pool, and the micro grooves suck the liquid to flow upwards to evaporate.

Most previous researches are focused on single, straight and inclined micro groove [1–6,8,9], and the circumferential micro groove has never been investigated. Therefore, this paper addresses the steady flow evaporation inside circumferential micro grooves with rectangular cross sections.

2. Physical model

An inclined circumferential micro groove on the outside surface of a heat transfer tube is sketched in Fig. 1, as well as the section 1-1 in breadth direction and 2-2 in axial direction.

When the bottom of the micro groove is immersed in a liquid pool, drawn by capillary suction force, the liquid will flow upwards along the groove against gravity and viscous friction. At the liquid entry, i.e. the point *I* in section 1-1, liquid full is usually assumed, thus, the dynamic contact angle there is 90°. The curvature of the

* Corresponding author. Tel./fax: +86 21 34206296.
E-mail address: xzz@sjtu.edu.cn (Z.Z. Xia).

0017-9310/$ - see front matter © 2008 Elsevier Ltd. All rights reserved.
doi:10.1016/j.ijheatmasstransfer.2008.05.041

Nomenclature

A	area (m^2), the lowest point in the intrinsic meniscus
$\overline{A}$	disjoining constant (J)
A–D	the four types of CV_{ij} at liquid–vapor interface
B	the joint of the intrinsic meniscus and evaporating thin film region
C	the joint of the evaporating thin film region and adsorbed region
$C1$, $C6$–$C7$	coefficients
$C9$–$C10$	coefficients
$C2$, $C3$–$C5$	exponents
$C8$	exponents
CV	control volume
D	groove depth (m)
D_1, D_2, D_i	diameter (m)
Gr	Grashof number
g	gravity acceleration (m/s^2)
h	heat transfer coefficient ($W/(m^2\,K)$)
$\bar{h}$	average heat transfer coefficient ($W/(m^2\,K)$)
h_{fg}	latent heat (kJ/kg)
I	groove liquid entry
int	integer
K	curvature (m^{-1})
k	parameter defined in (24) ($m^2\,s\,K\,kg^{-1}$)
l	the border lengths of control volumes, characteristic length (m), discrete number
M	molecular weight
m, n	discrete numbers
$\dot{m}$	evaporation mass flux ($kg/(m^2\,s)$)
Nu	Nusselt number
P	groove pitch (m)
Pe	ellipse perimeter (m)
Pr	Prandtl number
p	pressure (Pa)
Q	heat absorbing (W)
Q_1	heat absorbing in the extended meniscus (W/m)
Q_2	heat absorbing in the intrinsic region (W/m)
Q_3	heat absorbing in the evaporation thin film region (W/m)
q''	heat flux inside the tube (W/m^2)
q''_1, q''_2	heat flux (W/m^2)
R	universal gas constant (J/(mol K))
r	the radius of curvature (m)
s	groove liquid saturation
T	temperature (°C)
T_m	qualitative temperature (°C)
u	axial velocity (m/s)
$\bar{u}$	axial average velocity (m/s)
W	groove width (m)
x, y, z	coordinates (m)

Greek symbols

β	friction coefficient
δ	liquid film thickness (m)
δ_0	liquid film thickness in the adsorbed region (m)
ϕ_0	groove liquid entry coordinate (°)
ϕ	coordinate (m)
Γ_1	axial liquid flow rate (kg/s)
Γ_2	liquid flow rate inside the evaporation thin film region (kg/(m s))
η	coefficient of cubic expansion ($°C^{-1}$)
Λ	D/W
λ	thermal conductivity (W/(m K))
μ	viscosity (kg/(m s))
ν	dynamic viscosity (m^2/s)
Θ, ψ	the parameters defined in (9) dynamic contact angle (°)
ρ	density (kg/m^3)
$\sigma\overline{A}$	surface tension (N/m)
$\bar{\sigma}$	evaporation coefficient
ω	groove inclination angle (°)

Superscript

*	dimensionless

Subscipts

i	interface
Lower	under point I
l	liquid
loc	location
NC	natural convection
Supper	over point I
Total	whole groove
v	vapor
w	wall
∞	infinite

Others

I	the intrinsic meniscus
II	the evaporation thin film region
III	the adsorbed region
ΔT	degree of superheat (°C)
$\Delta y, \Delta z$	heat conduction distance (m)

curved liquid–vapor interface increases gradually with the liquid flow which, under the assumption of constant vapor pressure, will cause a gradually liquid pressure decrease. At the top of the micro groove, where the two pieces of liquids from the anterior and back groove meet and liquid velocities become zero, the curvature reaches a maximum value and the liquid pressure lowest. Such recession of the extended meniscus can be seen in section 1-1 where the thin solid line represents the positions of point A (in section 2-2, the lowest point at the curved liquid–vapor interface). For the groove inclination angle, ω, less than 90°, the section 1-1 features three ellipses those, from bigger to smaller, correspond to the top surface of the groove side wall, the groove bottom surface and the tube's inside surface, respectively. For small groove width (compared to the groove bottom diameter), the groove bottom line in section 2-2 can be treated as a straight line.

The minishing of the liquid film thickness between vapor and groove side wall will lead to a quick increase of disjoining pressure. The increase of disjoining pressure supplies a pressure gradient which drives the liquid film to flow upwards along the groove side wall (see Fig. 2). The whole extended meniscus is usually divided into three regions: the intrinsic meniscus, evaporation thin film region and adsorbed region those are marked by the signs III, II and I, respectively. In this model, the evaporation thin film region and adsorbed region are assumed to transform just at the top corner of the groove side wall. Thus, the top surface of the groove side wall is always covered by the adsorbed region. Due to the very thin liquid film thickness in the evaporation thin film region, the axial liquid flow inside which is restricted and can be neglected.

For the groove depth of 1.0 mm and side wall thickness of 0.15 mm, a temperature difference of 0.1 °C between side wall

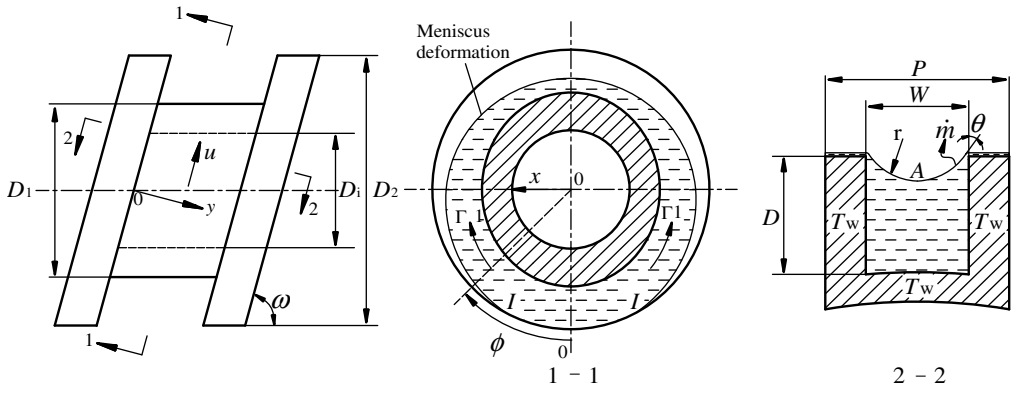

Fig. 1. The schematic of an inclined micro groove.

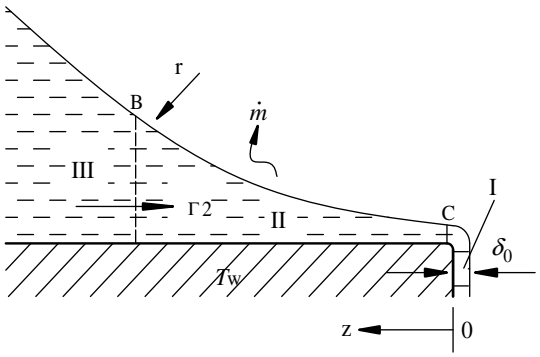

Fig. 2. The schematic of the extended meniscus.

bottom and top can support an average heat flux of 0.21 MW/m^2 given the contact angle of 30°. Generally, that heat flux is bigger than those of usual evaporators in refrigeration equipments. Therefore, the groove side wall temperature can be assumed to be constant.

Based on the above analysis, the following assumptions can be made:

(1) The vapor pressure and temperature are constant.
(2) The temperature of the groove wall is constant.
(3) The capillary flow analyzed in this paper is constrained to very small bond numbers, thus, the curvatures of the intrinsic meniscus for any axial section can be treated as constant.
(4) The liquid axial flow is constrained to the intrinsic meniscus and the region below it.
(5) The dynamic contact angle, θ, at the top of the heat transfer tube is bigger than, at least equals to, the minimum contact angle that means the absence of "corner flow".
(6) It is always at the top corners of the groove side walls where the evaporation thin film region and adsorbed region meet.

3. Mathematical model

The mathematical model is founded based on the coordinates ϕ, x, y and z. For the reason of symmetry, just the left part of the section 1-1 is modeled. The coordinate ϕ is the angle from the long axis of the outside ellipse to the section 2-2, and has a range of 0–π. The coordinate x starts from the center of the outside ellipse and goes leftwards along the short axis, it has a range of 0–$D_2/2$. For one point in the section 1-1, its coordinate x is determined by following way: draw an ellipse passing through the point, its long axis and short axis have the same ratios to those of the outside ellipse, the crossing point of the drawn ellipse and the x axial gives the point's x-coordinate. The coordinate y is perpendicular to the groove side walls and starts from the bottom of the left side wall which varies from 0 to the groove width W. The coordinate z starts from the top of the groove side wall and is contrary to the liquid film flow.

The whole-groove mathematical model composes the following five parts.

3.1. Natural convection

Under the groove liquid entry, i.e. point I, the heat transfer is characterized by natural convection for small degree of superheat. Due to very small groove depth, D, the enhancement effect of the micro grooves on the natural convection can be neglected. Therefore, a smooth outside surface of the heat transfer tube is assumed and the Nusselt number is given as [10]

$$Nu = C1 \cdot (Gr \cdot Pr)^{C2} \tag{1}$$

where the Grashof number $Gr = g\eta\Delta Tl^3/v^2$, the degree of superheat $\Delta T = T_w - T_\infty$, T_w and T_∞ are the groove wall temperature and the water temperature at infinite-far place, respectively, the coefficient of cubic expansion $\eta = 1/T_m$, the qualitative temperature $T_m = (T_w + T_\infty)/2$, the characteristic dimension l is chosen as D_2. For the laminar flow ($10^4 < Gr \cdot Pr < 1.5 \times 10^8$), $C1 = 0.48$ and $C2 = 0.25$.

The natural convection heat transfer coefficient, h_{NC}, can be calculated by

$$h_{NC} = Nu \cdot \lambda_l / D_2 \tag{2}$$

Thus, the heat absorbing under point I for one groove (just the left half of the section 1-1 in Fig. 1 is considered) is

$$Q_{Lower} = h_{NC} \cdot A_{NC} \cdot \Delta T \tag{3}$$

where A_{NC} is the heat transfer area based on the outside ellipse in the section 1-1 of Fig. 1 and calculated by

$$A_{NC} = \frac{1}{2} P \cdot D_2 \cdot \int_0^{\phi_0} \frac{1}{\sqrt{\sin^2\omega \sin^2\phi + \cos^2\phi}} \, d\phi \tag{4}$$

where P is the groove pitch, ϕ_0 is the coordinate of the groove liquid entry, ω is the groove inclination angle.

3.2. Liquid axial flow

For the liquid axial flow inside the groove, the continuity equation is given as

$$q''P = -\frac{4}{D_1 + D_2} \sqrt{\frac{tg^2\phi + \sin^2\omega}{1 + tg^2\phi}} \frac{d\Gamma_1}{d\phi} h_{fg} \tag{5}$$

where q'' is the heat flux inside the tube, W/m^2, Γ_1 is the axial liquid flow rate, kg/s and is calculated by

$$\Gamma_1 = \rho \bar{u} W D s \tag{6}$$

where $\bar{u}$ is the liquid average axial velocity, m/s. For an inclined groove, the groove depth, D, is related to ϕ by

$$D = \frac{D_2 - D_1}{2}\sqrt{\frac{1 + tg^2\phi}{tg^2\phi + \sin^2\omega}} \tag{7}$$

The sign "s" in Eq. (6) denotes the groove liquid saturation. Neglecting the area occupied by the evaporation thin film region, s can be calculated by

$$s = 1 - \frac{1}{\Lambda \cos^2\theta}\left(\frac{\pi}{8} + \frac{\theta}{4} + \frac{\sin\theta\cos\theta}{4}\right) \tag{8}$$

where Λ represents the ratio of D/W.

The viscous friction force between the liquid and groove wall, $\beta\mu\bar{u}/W^2$, the gravitational force acting along the axial tangent of the groove bottom surface and the gradient of the liquid pressure, p_l are balanced by

$$\frac{\beta\mu\bar{u}}{W^2} + \rho g \sin\omega \sin\phi + \frac{4}{D_1 + D_2}\sqrt{\frac{tg^2\phi + \sin^2\omega}{1 + tg^2\phi}}\frac{dp_l}{d\phi} = 0 \tag{9}$$

where β is the friction coefficient and is given by the literature [9]

$$\beta = 1\Bigg/\left[\frac{0.083^{C3}\left[\left(\frac{1}{C6\cdot\psi+3\psi^2}\right)^{C5} + \left[\frac{0.0027^{C4}}{1+0.0027^{C4}\left[7(\Theta-2)^2+C7\cdot(\Theta-2)^{C8}\right]^{C4}}\right]^{C5/C4}\right]^{C3/C5}}{0.083^{C3} + \left[\left(\frac{1}{C6\cdot\psi+3\psi^2}\right)^{C5} + \left[\frac{0.0027^{C4}}{1+0.0027^{C4}\left[7(\Theta-2)^2+C7\cdot(\Theta-2)^{C8}\right]^{C4}}\right]^{C5/C4}\right]^{C3/C5}}\right]^{1/C3} \tag{10}$$

where $\psi = \frac{2\cos\theta}{2\Lambda\cos\theta + \sin\theta - 1}$ and $\Theta = \frac{2\cos\theta}{1-\sin\theta}$. The exponents $C3$–$C5$ and $C8$ are 1.31, 1.88, 0.82 and 0.87, respectively, the coefficients $C6$–$C7$ are 2.6 and 150, respectively. For one given groove, the coefficient β is determined only by θ.

3.3. The heat transfer in and below the intrinsic meniscus

This region includes two parts: the intrinsic meniscus and the region below it inside the groove. For micro groove, convection heat transfer is constrained and pure heat conduction can be assumed. The cross section 2-2 in Fig. 1 is symmetrical in shape, thus only one half is chosen to be analyzed. For an axial cross section, the discrete left half is sketched in Fig. 3. Along coordinate y, the discrete region is from $y = 0$ to $y = W/2$ and the discrete number is m. Along coordinate z, the discrete region is from $z = z_B$ to $z = D$ and the discrete number is n. The discrete numbers m and n can be adjusted according to the required accuracy. For control region CV_{jk}, assuming constant thermal properties, there has energy conservation equation

$$\frac{\lambda l_{\text{Left}}(T_{j-1,k} - T_{j,k})}{\Delta y} + \frac{\lambda l_{\text{lower}}(T_{j,k-1} - T_{j,k})}{\Delta z} = \frac{\lambda l_{\text{right}}(T_{j,k} - T_{j+1,k})}{\Delta y} + \frac{\lambda l_{\text{upper}}(T_{j,k} - T_{j,k+1})}{\Delta z} + \dot{m}\cdot\widehat{45}\cdot h_{fg} \tag{11}$$

where λ is the liquid thermal conductivity, W m^{-2} K^{-1}, the heat transfer distances Δy and Δz equal to $W/(2m)$ and $(D - z_B)/n$, respectively, l_{lower}, l_{upper}, l_{left} and l_{right} are the border lengths of the control region CV_{jk}, m, h_{fg} is the evaporation latent heat, kJ/kg, $\dot{m}$ is the evaporation mass flux at the curved liquid–vapor interface and is given below

$$\dot{m} = C9\cdot(T_i - T_v) + C10\cdot(p_l - p_v) \tag{12}$$

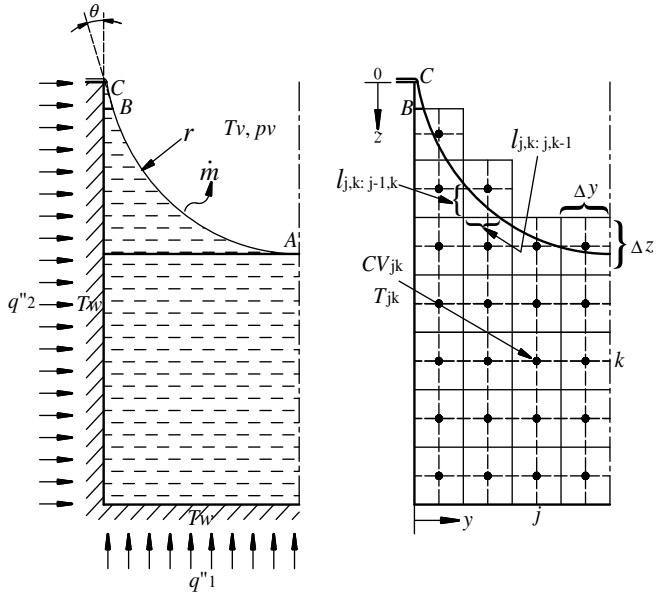

Fig. 3. The discrete schematic for the intrinsic meniscus region and the region below it.

where the coefficients $C9$ and $C10$ depend on the liquid thermal properties only and can be calculated. The term "$p_l - p_v$" is the pressure drop across the curved liquid–vapor interface and can be calculated by

$$p_l - p_v = -\sigma K + \frac{\overline{A}}{\delta^3} \tag{13}$$

where σ denotes the liquid surface tension, N/m, K the curvature of the curved liquid–vapor interface, 1/m, $\overline{A}$ the disjoining force, J, δ the liquid film thickness, m. For the intrinsic meniscus, the item $\overline{A}/\delta^3$ can be neglected compared to $-\sigma K$.

For the control regions at the liquid–vapor interface, there have four cases, i.e. types A–D in Fig. 4. The curved liquid–vapor interface can be formulated by the following equations:

$$y = f(z) = \frac{W}{2} - \frac{1}{2}\sqrt{\frac{(W - 2\delta_B)^2}{\cos^2\theta} - [2z - 2z_B + (W - 2\delta_B)tg\theta]^2} \tag{14a}$$

or

$$z = g(y) = z_B - \frac{(W - 2\delta_B)tg\theta}{2} + \frac{1}{2}\sqrt{\frac{(W - 2\delta_B)^2}{\cos^2\theta} - (W - 2y)^2} \tag{14b}$$

The control region where point (y,z) locates is decided by

$$j = \text{int}\left(\frac{2my}{W}\right) + 1 \tag{15a}$$

$$k = \text{int}\left(\frac{n(D - z)}{D - z_B}\right) + 1 \tag{15b}$$

Types A–D are identified by Eqs. (16a)–(16d), respectively:

$$\text{int}\left(\frac{f(D - k\Delta z)}{\Delta y}\right) = j - 1, \quad \text{int}\left(\frac{D - g(j\Delta y)}{\Delta z}\right) = k - 1 \tag{16a}$$

$$\text{int}\left(\frac{f(D - k\Delta z)}{\Delta y}\right) = j - 1, \quad \text{int}\left(\frac{f(D - (k-1)\Delta z)}{\Delta y}\right) = j - 1 \tag{16b}$$

$$\text{int}\left(\frac{D - g[(j-1)\Delta y]}{\Delta z}\right) = k - 1, \quad \text{int}\left(\frac{D - g(j\Delta y)}{\Delta z}\right) = k - 1 \tag{16c}$$

$$\text{int}\left(\frac{f(D - (k-1)\Delta z)}{\Delta y}\right) = j - 1, \quad \text{int}\left(\frac{D - g[(j-1)\Delta y]}{\Delta z}\right) = k - 1 \tag{16d}$$

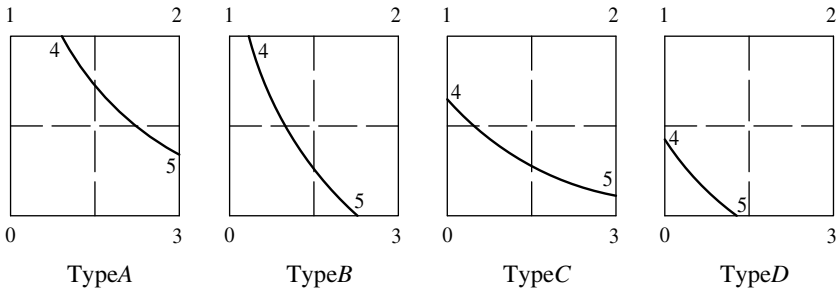

Fig. 4. The four cases at the curved liquid–vapor interface.

In Eq. (10), the item 45 represents the arc length of the curved liquid–vapor interface of the control region CV_{jk}. For type *A*, the border lengths of the control region are calculated by

$$l_{1-4} = f(D - k\Delta z) - (j-1)\Delta y \tag{17a}$$
$$l_{3-5} = D - (k-1)\Delta z - g(j\Delta y) \tag{17b}$$
$$\widehat{45} = \frac{W - 2\delta_B}{\cos\theta} \times \arcsin\left(\frac{\cos\theta\sqrt{[f(D-k\Delta z) - j\Delta y]^2 + [D - k\Delta z - g(j\Delta y)]^2}}{W - 2\delta_B}\right) \tag{17c}$$

For type *B*

$$l_{1-4} = f(D - k\Delta z) - (j-1)\Delta y \tag{18a}$$
$$l_{0-5} = f[D - (k-1)\Delta z] - (j-1)\Delta y \tag{18b}$$
$$\widehat{45} = \frac{W - 2\delta_B}{\cos\theta} \times \arcsin\left(\frac{\cos\theta\sqrt{\{f(D-k\Delta z) - f[D-(k-1)\Delta z]\}^2 + (\Delta z)^2}}{W - 2\delta_B}\right) \tag{18c}$$

For type *C*

$$l_{0-4} = D - (k-1)\Delta z - g((j-1)\Delta y) \tag{19a}$$
$$l_{3-5} = D - (k-1)\Delta z - g(j\Delta y) \tag{19b}$$
$$\widehat{45} = \frac{W - 2\delta_B}{\cos\theta} \times \arcsin\left(\frac{\cos\theta\sqrt{(\Delta y)^2 + \{g[(j-1)\Delta y] - g(j\Delta y)\}^2}}{W - 2\delta_B}\right) \tag{19c}$$

For type *D*

$$l_{0-4} = D - (k-1)\Delta z - g((j-1)\Delta y) \tag{20a}$$
$$l_{0-5} = f(D - (k-1)\Delta z) - (j-1)\Delta y \tag{20b}$$
$$\widehat{45} = \frac{W - 2\delta_B}{\cos\theta} \arcsin\left(\frac{\cos\theta\sqrt{\{(j-1)\Delta y - f[D-(k-1)\Delta z]\}^2 + \{g[(j-1)\Delta y] - D + (k-1)\Delta z\}^2}}{W - 2\delta_B}\right) \tag{20c}$$

For Eq. (11), the boundary conditions are listed below

$$T_{1,k} = T_w \quad k = 1\text{–}n \tag{21a}$$
$$T_{j,1} = T_w, \quad j = 1\text{–}m \tag{21b}$$

For $j = m$

$$l_{right} = 0 \tag{21c}$$

For inside control volumes, the arc length 45 is zero. The liquid film thickness δ in the intrinsic meniscus region can be calculated by

$$\delta = \delta_B + \frac{(z - z_B)^2}{W - 2\delta_B} + (z - z_B)tg\theta \tag{22}$$

where δ_B is the liquid film thickness at point *B* (see Fig. 2) that is the joint of the intrinsic meniscus and evaporation thin film region. At point *A* (Fig. 1), the liquid film thickness reaches maximum and equals to $W/2$. Substitute $\delta = W/2$ into Eq. (22), the *z*-coordinate of point *A* can be obtained. The heat absorbing in the intrinsic meniscus can be calculated by

$$Q_2 = 2\int_{z_B}^{z_A} \dot{m} h_{fg}\, dz \tag{23}$$

3.4. The evaporation thin film region

In this region, δ decreases quickly along negative *z*-coordinate direction, as well as the film thickness gradient, $d\delta/dz$. Therefore, with the liquid film flow, the term $-\overline{A}/\delta^3$ in Eq. (13) will increase and exceed the term σK quickly. For the most part of the evaporation thin film region, σK is much lower than $-\overline{A}/\delta^3$ and can be neglected. And Eq. (13) can be simplified to

$$p_l - p_v = \frac{\overline{A}}{\delta^3} \tag{24}$$

The evaporation thin film region has been investigated by many researchers, and many physical and mathematical models have been presented [11–16]. Among those, the model built by Schonberg and Wayner Jr. [14] has been referred to widely. Some key equations in that model are given below.

The liquid film thickness δ can be deduced as a function of *z*-coordinates

$$-3\frac{1}{\delta^*}\frac{d\delta^*}{dz^*} = \left[18(1+k^3)\ln\left[\frac{\delta^*(1+k)}{1+k\delta^*}\right] + 6\left[\left(\frac{1}{\delta^*}\right)^3 - 1\right] + 9k\left[1 - \left(\frac{1}{\delta^*}\right)^2\right] + 18k^2\left(\frac{1}{\delta^*} - 1\right)\right]^{1/2} \tag{25}$$

where *k* represents a combination of $C9 \cdot h_{fg}\delta_0/\lambda$, δ_0 is the liquid film thickness in the adsorbed region and will be given lately. The dimensionless liquid film thickness, δ^*, and dimensionless *z*-coordinates, z^*, are defined by Eqs. (26) and (27), respectively

$$\delta^* = \delta/\delta_0 \tag{26}$$
$$z^* = z\Big/\left(-\frac{\overline{A}}{C9 \cdot \Delta T \cdot \nu_l}\right)^{1/2} \tag{27}$$

where ν_l is the kinetic viscosity, $m^2\,s^{-1}$.

The dimensionless local heat transfer coefficient h^*_{loc} is defined by $h_{loc}/C9/h_{fg}$ and can be calculated by

$$h^*_{loc} = \frac{1-(\delta^*)^{-3}}{1+k\delta^*} \tag{28}$$

The dimensionless average heat transfer coefficient $\bar{h}(\delta)^*$ from point C (Fig. 2) to the point with the liquid film thickness of δ is calculated by

$$\bar{h}(\delta)^* = \frac{\int_1^{\delta^*} h^*_{loc}\,d\delta^*}{\int_1^{\delta^*} d\delta^*} = \frac{1}{\delta^*-1}\left\{\frac{1}{k}\ln\left(\frac{k\delta^*+1}{k+1}\right) - k^2\ln\left(\frac{(k+1)\delta^*}{k\delta^*+1}\right) - \frac{2k\delta^*-1}{2(\delta^*)^2} + k - \frac{1}{2}\right\} \tag{29}$$

Given the heat absorbing in the evaporation thin film region, Q_3, the z-coordinates of point B, z_B, can be calculated by

$$z_B = \frac{Q_3}{2\bar{h}(\delta_B)\Delta T} \tag{30}$$

3.5. The adsorbed region

In this region, due to ultra-small thickness, the liquid film is adsorbed to the solid surface.

Though the liquid film is superheated, no evaporation occurs. Therefore, the evaporation mass flux, as well as the curvature of the liquid–vapor interface, is zero, and the liquid film thickness δ_0 can be calculated by

$$\delta_0 = \left(\frac{-C10\cdot\bar{A}}{C9\Delta T}\right)^{1/3} \tag{31}$$

The total heat absorbing in the extended meniscus, Q_1, is given by

$$Q_1 = q''P = Q_2 + Q_3 \tag{32}$$

For the groove part over point I, the total heat absorbing, Q_{Upper}, can be calculated by

$$Q_{Upper} = \int_{\phi_0}^{\pi} q''P\frac{D_i}{2}\sqrt{\frac{1+tg^2\phi}{tg^2\phi+\sin^2\omega}}\,d\phi \tag{33}$$

where ϕ_0 is the ϕ-coordinates of point I. Combine the capillary-assisted evaporation and natural convection heat transfer, the total heat absorbing for the half groove ($\phi = 0$–π), Q_{Total}, can be obtained by

$$Q_{Total} = Q_{Upper} + Q_{Lower} \tag{34}$$

The whole-groove equivalent evaporation heat transfer coefficient can be obtained by

$$h_{Total} = \frac{Q_{Total}}{A_{Total}\Delta T} \tag{35}$$

where the total heat transfer area of the half groove ($\phi = 0$–π), A_{Total}, is calculated by

$$A_{Total} = Pe\cdot P/2 \tag{36}$$

Due to symmetrical in shape, the other half of the groove has the same characters, i.e. the model based on the half groove can predict the whole one.

4. Solution strategy

The known parameters in the model are the groove geometric parameters, liquid categories, groove liquid entry, evaporating pressure, degree of superheat, etc. The parameters to be solved include the liquid–vapor interface profiles at different ϕ-coordinates, the whole-groove equivalent heat transfer coefficient, etc. For the natural convection heat transfer under the groove liquid entry, the temperature T_∞ is assumed to be equal to the evaporation saturated temperature that relates to the evaporating pressure. For the groove part over the liquid entry where the heat transfer is characterized by the capillary-assisted evaporation, the range $\phi = \phi_0$–π is divided evenly into l shares. Firstly, a set of heat flux q''s are guessed, and, with q'' and other known parameters, the θs of the discrete units in ϕ-direction can be obtained. For any ϕ-directional discrete unit, with θ and other known parameters, the intrinsic meniscus and evaporation thin film region can be solved. Thus, the heat absorbing in the two regions, i.e. Q_2 and Q_3, as well as Q_1, can be obtained. Hence, a new set of heat flux $(q'')'$ can be obtained. Compare q'' and $(q'')'$, if the departure equals or is smaller than the permitted error set previously, the calculating stops. Otherwise, replacing q'' with $(q'')'$, the above steps are followed again.

5. Solution results and discussions

5.1. Dynamic contact angle

Dynamic contact angle θ is a very important parameter affecting the heat absorbing in the intrinsic meniscus and evaporation thin film region, as well as the liquid–vapor interface profile of the extended meniscus. For a given ϕ, θ is related to the groove geometric parameters, ϕ_0, the evaporating pressure, p_v, the liquid thermal physical properties, etc.

(1) Dynamic contact angle and the heat absorbing in the intrinsic meniscus: The variation of the heat absorbing in the intrinsic meniscus, Q_2, with θ is given in Fig. 5. The evaporating liquid is chosen as methanol, the computational parameters are P = 0.5 mm, W = 0.2 mm, D = 0.5 mm, and the evaporating saturated temperature T_e = 5 °C. From the figure we can see that Q_2 decreases quickly with θ, and a higher ΔT leads to a larger Q_2. For ΔT = 4 °C, when θ increases from 30° to 85°, Q_2 decreases from 9.2 to 0.47 W m^{-1}. The reason is that the liquid–vapor interface area, i.e. the mass transfer area, decreases with θ increasing.

(2) Dynamic contact angle and the heat absorbing in the evaporation thin film region: For point B, $d\delta/dz = tg\theta$ is satisfied. Thus, a bigger θ will result in a larger $d\delta/dz$. The larger $d\delta/dz$ is, the bigger disjoining force gradient can be obtained which can drive more liquid to flow into the evaporation thin film region. So, under the

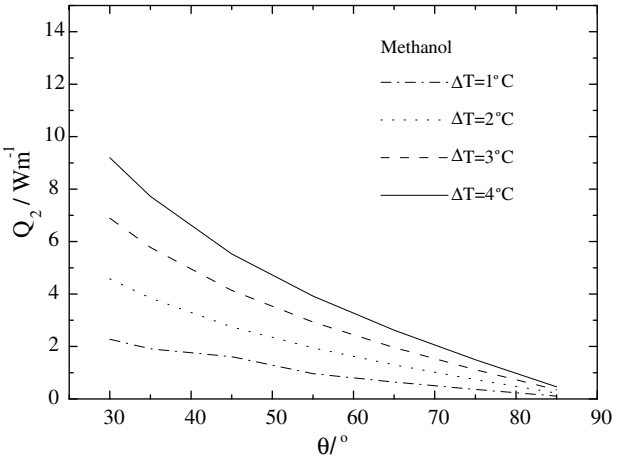

Fig. 5. The variation of Q_2 with θ for different ΔT.

same ΔT, the heat absorbing in the evaporating thin film region, Q_3, increases with θ that is shown in Fig. 6. Compare Figs. 5 and 6, it can be seen that Q_2 is much larger than Q_3 when θ is small. However, the difference between the two becomes smaller and smaller when θ increases, and they are equivalent when θ reaches around 80°.

(3) The influence of groove liquid entry on dynamic contact angle: From Fig. 1 we can see that the liquid enters the groove at point *I* and flows upwards to the groove top surface. The lower point *I* is, i.e. the smaller ϕ_0 is, the liquid flow distance inside the groove is longer which needs a bigger driving force. Therefore, at a given ϕ, θ must decrease to produce a larger surface tension force, i.e. a bigger liquid pressure gradient to drive the liquid flow. Introduce dimensionless $\phi^* = \phi/\pi$, the variation of θ with ϕ_0^* is shown in Fig. 7. The computational parameters are $P = 0.5$ mm, $W = 0.2$ mm, $D_1 = 18$ mm, $D = 0.5$ mm, $\omega = 90°$, $T_e = 5$ °C, $\Delta T = 2$ °C. From the figure we can see that, at the same ϕ, θ decrease evidently when ϕ_0^* decrease.

(4) The influence of groove bottom diameter on dynamic contact angle: The groove bottom diameter, D_1, has a similar effect on θ as ϕ_0. The bigger D_1 is, the longer the liquid flow distance is from point *I* to the groove top surface which needs a bigger driving force. Therefore, θ has a negative relation to D_1 that is shown in Fig. 8 ($\phi_0^* = 1/2$). The computational parameters are $P = 0.5$ mm, $W = 0.2$ mm, $D = 0.5$ mm, $\omega = 90°$, $T_e = 5$ °C, $\Delta T = 2$ °C, $\phi_0^* = 1/2$.

(5) The influence of the groove inclination angle on θ: Through the dimension analysis on Eq. (9), we can know that, for methanol, the gravity term $\rho g \sin\omega \sin\phi$ is much bigger than the viscosity term $\beta\mu\bar{u}/W^2$. Therefore, when ω decreases, $\rho g \sin\omega \sin\phi$ decreases which will reduce the liquid flow resistance. Fig. 9 offers the relationship between ω and θ. The computational parameters are $P = 0.5$ mm, $W = 0.2$ mm, $D_1 = 18$ mm, $D = 0.5$ mm, $T_e = 5$ °C, $\Delta T = 2$ °C, $\phi_0^* = 1/2$.

5.2. The whole-groove equivalent heat transfer coefficient

For a micro groove partly immersed into liquid, driven by ΔT, the capillary-assisted evaporation will occur over the liquid entry, and natural convection under the liquid entry. Therefore, combining the two, for the whole groove, an equivalent heat transfer coefficient exists that can be calculated by Eqs. 3 and (33)–(35). The whole-groove equivalent heat transfer coefficient, h_{Total} is affected strongly by some factors such as the groove liquid entry, evaporating pressure, degree of superheat, groove inclination angle, bottom diameter, etc.

(1) The groove liquid entry: Compare to natural convection, capillary-assisted evaporation heat transfer has a much higher efficiency. Thus, the bigger the groove part over the liquid entry is, the higher h_{Total} is. Fig. 10 shows the dependency of h_{Total} on ϕ_0^*. The other parameters are $P = 0.5$ mm, $W = 0.2$ mm, $D_1 = 18$ mm, $D = 0.4$ mm, $\omega = 90°$. In Fig. 10, the smallest ϕ_0^* equals 0.33, and the biggest equals 1. From the figure we can see that an increase of h_{Total} from 2600 W/(m^2 K) to nearly 6000 W/(m^2 K) can be obtained when ϕ_0^* decreases from 0.67 to 0.33. For $\phi_0^* = 1$, the whole

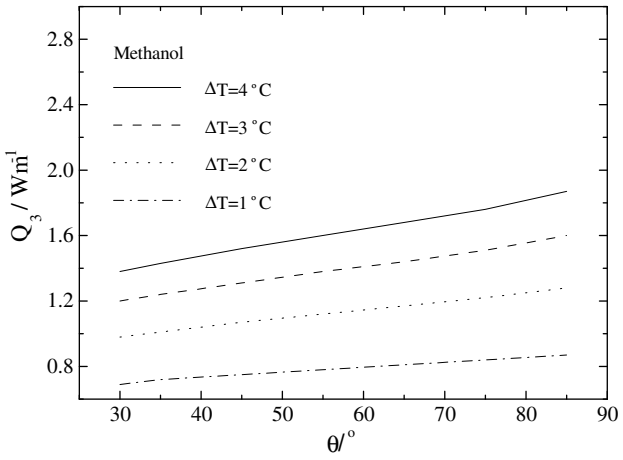

Fig. 6. The variation of Q_3 with θ for different ΔT.

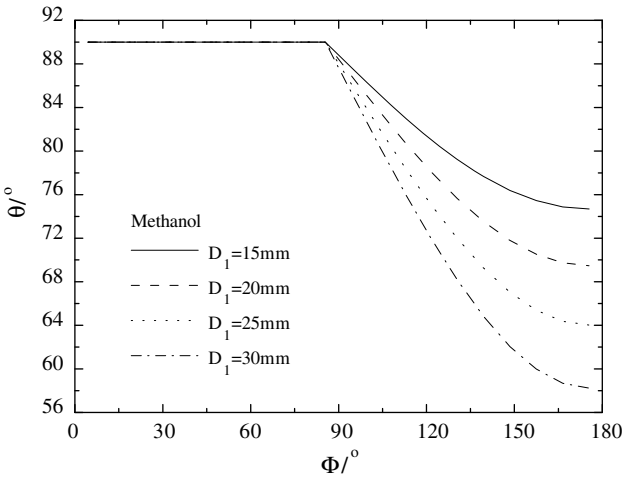

Fig. 8. The variation of θ with ϕ for different D_1.

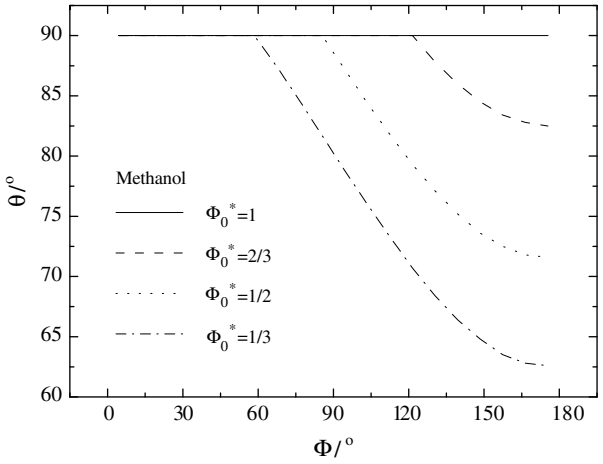

Fig. 7. The variation of θ with ϕ for different ϕ_0^*.

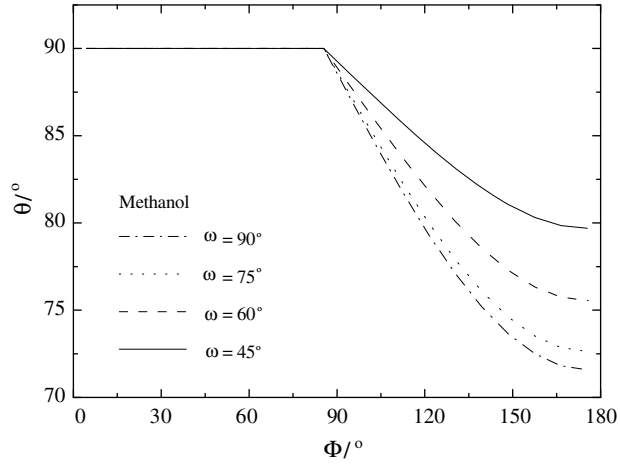

Fig. 9. The variations of θs with ϕs for different ω.

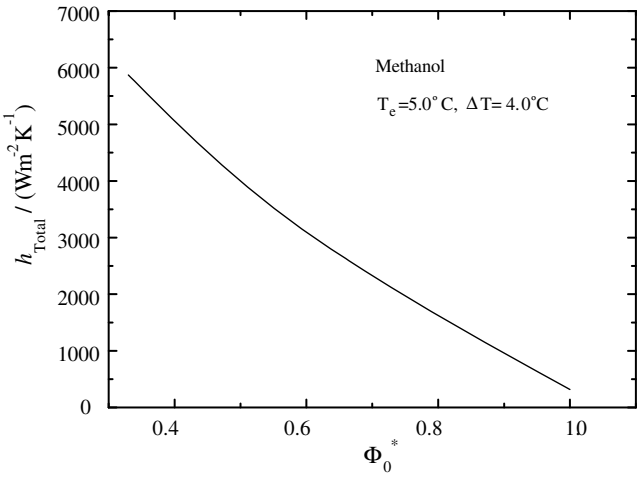

Fig. 10. The variation of h_{Total} with ϕ_0^*.

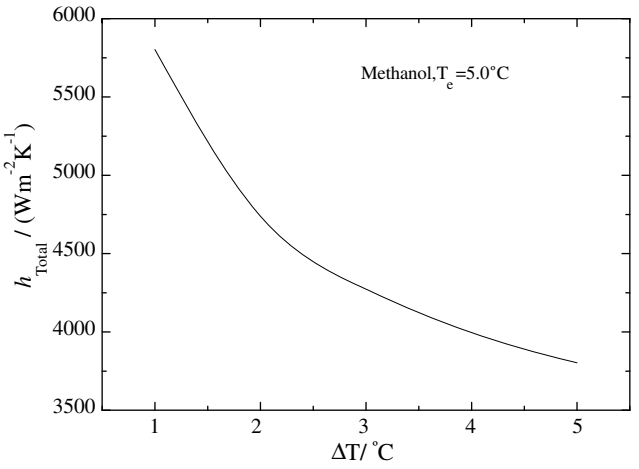

Fig. 12. The variation of h_{Total} with ΔT.

groove is characterized by natural convection heat transfer, so, only 320 W/(m^2 K) of h_{Total} can be obtained.

(2) The evaporating pressure: For constant ΔT, the higher the evaporating pressure is, the higher the liquid film temperature is, which in turn increases the liquid thermal conductivity and decreases viscosity. Therefore, an increase of h_{Total} can be anticipated. The variation of h_{Total} with the evaporation saturated temperature, T_e, is presented in Fig. 11. When T_e increases from 5 to 15 °C, h_{Total} increases from 4400 to 4900 W/(m^2 K). The other parameters are P = 0.5 mm, W = 0.2 mm, D_1 = 18 mm, D = 0.4 mm, ω = 90°, $\phi_0^* = 0.5$.

(3) The degree of superheat: The liquid film temperature increases with increasing ΔT and constant T_e. Similar to the evaporating pressure increasing, it can increase the liquid thermal conductivity and decrease viscosity. However, with ΔT increasing, the heat flux across the liquid film will increase quickly, and the liquid film will also become thicker quickly that will increase the heat conduction resistance. The variation of h_{Total} with ΔT is given in Fig. 12. It is shown that h_{Total} decreases from 5800 to 3800 W/(m^2 K) when ΔT increases from 1 to 5 °C. The other parameters are P = 0.5 mm, W = 0.2 mm, D_1 = 18 mm, D = 0.4 mm, ω = 90°, $\phi_0^* = 0.5$. It also indicates that the heat conduction resistance inside the liquid film plays an important role in the whole thermal resistance.

(4) The groove inclination angle: It has been analyzed above that the decrease of ω will cause θ increasing (see Fig. 9). Though a bigger θ is preferred for the heat absorbing in the evaporation thin film region, the heat absorbing in the intrinsic meniscus, Q_2, will decrease (see Figs. 5 and 6). Therefore, under constant other conditions, the decrease of ω will produce a negative impact on h_{Total}, as shown in Fig. 13. The other parameters are P = 0.5 mm, W = 0.2 mm, D_1 = 18 mm, D = 0.4 mm, $\phi_0^* = 0.5$. The figure indicates that h_{Total} will increase from 3600 to 4300 W/(m^2 K) when ω increases from 50° to 90°. Hence, a bigger ω is desired to improve h_{Total}.

(5) The groove bottom diameter: According to the above analysis, for the same ϕ, a bigger D_1 will lead to a smaller θ. Therefore, the increase of D_1 will have a positive effect on h_{Total}. The variation of h_{Total} with D_1 is presented in Fig. 14. h_{Total} increases from 4000 to 5100 W/(m^2 K) when D_1 increases from 15 mm to 30 mm. The other parameters are P = 0.5 mm, W = 0.2 mm, D = 0.4 mm, ω = 90°, $\phi_0^* = 0.5$. However, D_1 cannot be increased unlimitedly because "corner flow" may appear if D_1 is too large.

(6) The groove depth: The groove depth D can affect the capillary-assisted evaporation heat transfer through three ways. Firstly, under constant D_1, P and W, the liquid flow friction force inside the groove increases with D which requires a bigger driving force, i.e. a larger gradient of θ. Secondly, the variation of D will change the relation between θ and the groove liquid saturation, s. Finally, with D decreasing, the distance from the groove bottom surface to the liquid–vapor interface decreases. If that distance decreases to the same order as the liquid film thickness in the intrinsic meniscus, the heat conduction from the groove bottom-wall to the liquid–vapor interface must be considered. The variation of h_{Total} with Λ is shown in Fig. 15. It can be seen that h_{Total} reaches the smallest

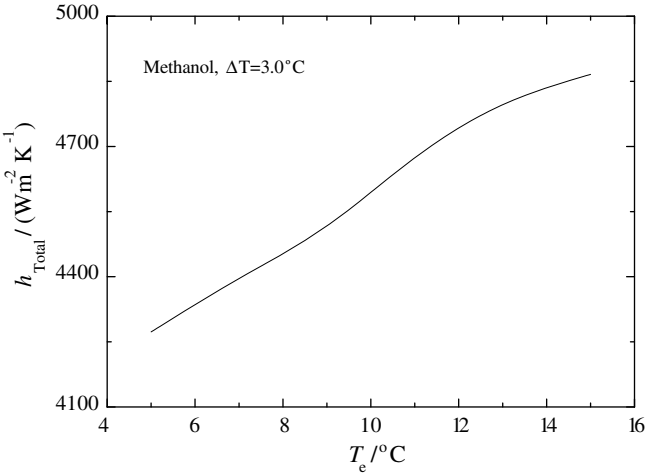

Fig. 11. The variation of h_{Total} with T_e.

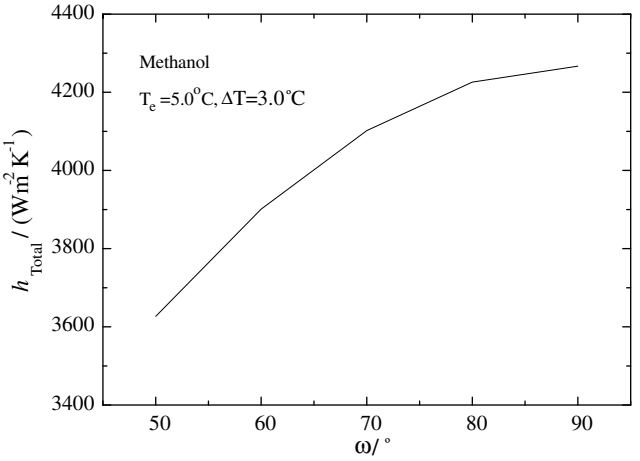

Fig. 13. The variation of h_{Total} with ω.

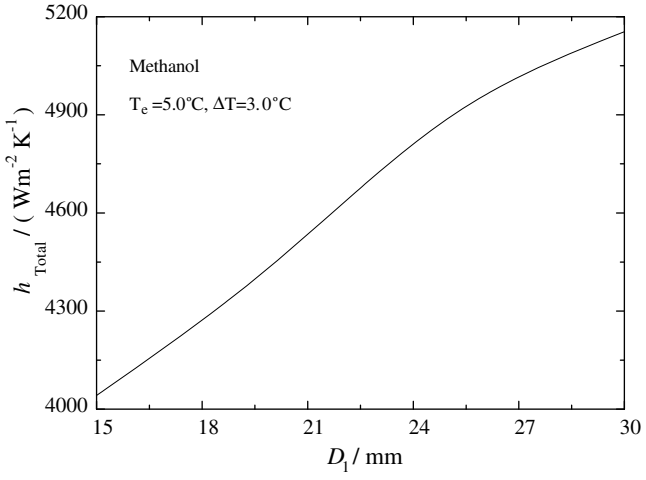

Fig. 14. The variation of h_{Total} with D_1.

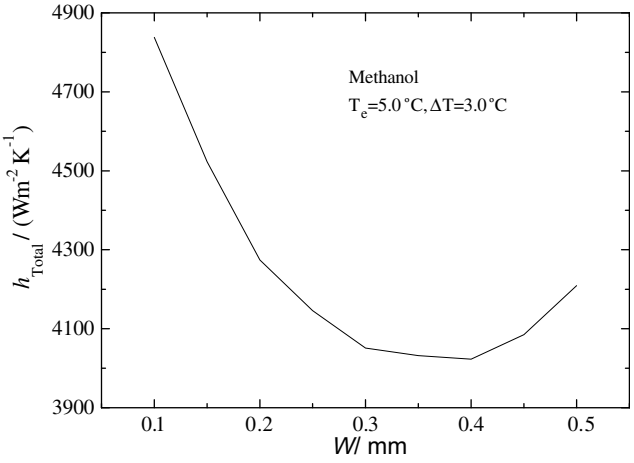

Fig. 16. The variation of h_{Total} with W.

at $\Lambda = 2$ ($D = 0.4$ mm). The other parameters are $P = 0.5$ mm, $W = 0.2$ mm, $D_1 = 18$ mm, $\omega = 90°$, $\phi_0^* = 0.5$. Though the decrease of Λcan increase h_{Total} when $\Lambda < 2$, "dead zone" and "corner flow" are more possible to occur. Hence, Λ cannot be too small. When $\Lambda > 2$, a bigger Λ is benefit to get a higher h_{Total}, but, the groove machine becomes more and more difficult with Λ increasing. So, the determination of Λ in actual application should consider the above factors synthetically.

(7) The groove width: Under constant D_1, D and the groove side wall thickness, i.e. $(P - W)/2$, a bigger W means more liquid inside the groove needed to be driven. Hence, the θ under bigger W should be smaller. However, the bigger W is, the larger the heat transfer area is which can bring a negative effect on h_{Total} according to Eq. (35). Fig. 16 presents the variation of h_{Total} with W. From the figure we can see that there exists an inflexion ($W = 0.4$) on the curve where h_{Total} reaches lowest. The other parameters are $D_1 = 18$ mm, $D = 0.5$ mm, $(P - W)/2$=0.15 mm, $\omega = 90°$, $\phi_0^* = 0.5$. Similar to D, the choice of W should also consider groove machine and the possibilities of "dead zone" and "corner flow" occurring.

6. Comparison with experiments and other models

The literature [17] has carried out the capillary-assisted evaporation experiment on the outside surfaces of some enhanced tubes. For validating the mathematical model built in this paper, the experimental results of the tube with $W = 0.2$ mm, $D = 1.0$ mm, $D_1 = 17.0$ mm and $\omega = 90°$ are chosen to be compared with the calculated results. The mathematical model in the literature [9], in which the heat absorbed in the evaporation thin film region was neglected, and [7], in which both the evaporation thin film region and gravity are not considered, are also quoted here for comparison. The comparison results are shown in Fig. 17. The calculated dimensionless coordinates $\phi_0^* = 0.5$, $\Delta T = 3.0$ °C, the experimental $\phi_0^* = 0.5 \pm 0.017$, $\Delta T = 3.0 \pm 0.2$ °C. It indicates that an obvious underestimate has been caused by neglecting the heat absorbed in the evaporation thin film region. The calculated results by the model built in this paper agree with the experimental results in [17] very well.

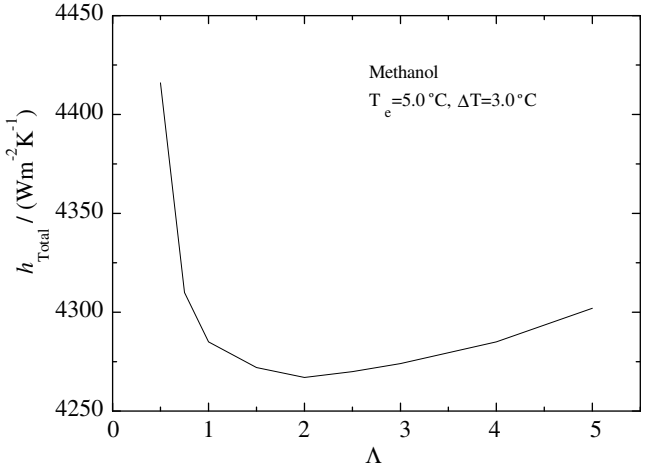

Fig. 15. The variation of h_{Total} with Λ.

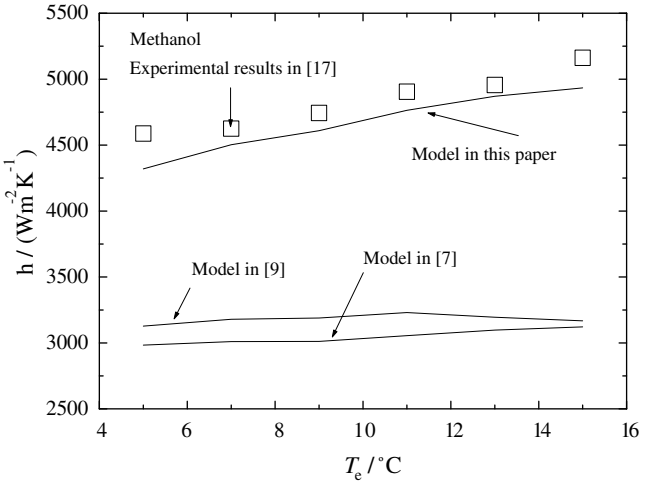

Fig. 17. The comparisons of the model in this paper with existing models [7,9] and the experimental results [17].

7. Conclusions

Aiming at introducing the capillary-assisted evaporation from micro-size fields to normal-size fields, this paper has developed a systematic model on an inclined circumferential groove with rectangular cross sections. In the model, both the intrinsic meniscus and evaporation thin film region are considered when calculating the heat absorbing at the groove axial cross section. For the intrin-

sic meniscus, the liquid temperature and, then, the evaporating mass flux at the liquid–vapor interface can be obtained by solving the heat transfer model in and below the intrinsic meniscus. For the evaporation thin film region, a classic model from the literature [14] is used to describe the heat and mass transfer. Through solving the model built in this paper, the following conclusions can be made:

(1) With θ increasing, the heat absorbing in the intrinsic meniscus, Q_2, decreases, and that in the evaporation thin film region, Q_3, increases. For small θ, Q_3 can be ignored compared to Q_2. But, the difference between the two decreases quickly with θ increasing. For the given parameters in this paper, Q_2 and Q_3 will reach the same order when θ accesses 70°. Therefore, Q_3 must be considered for big θ.
(2) For the same ϕ, θ increases with the groove liquid entry, ϕ_0, increasing, the groove bottom diameter, D_1, decreasing and the groove inclination angle, ω, decreasing.
(3) The whole-groove equivalent heat transfer coefficient, h_{Total}, is related closely with ϕ_0, the evaporating pressure and the degree of superheat, ΔT. For the groove with $P = 0.5$ mm, $W = 0.2$ mm, $D_1 = 18$ mm, $D = 0.4$ mm, $\omega = 90°$ and the evaporating liquid of methanol, h_{Total} will increase from 2600 W/(m^2 K) to nearly 6000 W/(m^2 K) when ϕ_0^* decreases from 0.67 to 0.33 ($T_e = 5$ °C, $\Delta T = 4$ °C). If ϕ_0^* is fixed at 0.5 and $T_e = 5$ °C, h_{Total} will decrease from 5800 to 3800 W/(m^2 K) when ΔT increases from 1 to 5 °C. If ΔT is fixed at 3 °C and $\phi_0^* = 0.5$, h_{Total} will increase from 4400 to 4900 W/(m^2 K) when T_e increases from 5 to 15 °C.
(4) The groove bottom diameter, D_1, and the groove inclination angle, ω, also offer strong effects on h_{Total}. For methanol, the groove with $P = 0.5$ mm, $W = 0.2$ mm, $D = 0.4$ mm, $\omega = 90°$ and $\phi_0^* = 0.5$, $T_e = 5$ °C, $\Delta T = 3$ °C, h_{Total} will increase from 4000 to 5100 W/(m^2 K) when D_1 increases from 15 to 30 mm. If D_1 is fixed at 18 mm, h_{Total} will increase from 3600 to 4300 W/(m^2 K) when ω increases from 50° to 90°.
(5) The groove geometric parameters have also effects on h_{Total}. No monotonic relationship is found between h_{Total} and W, h_{Total} and D.

Acknowledgement

This work was supported by the National 863 Program (Hi-Tech Research and Development Program of China) under the contract No. 2006AA05Z413.

References

[1] G.P. Peterson, H.B. Ma, Theoretical analysis of the maximum heat transport in triangular grooves: a study of idealized micro heat pipes, ASME J. Heat Transfer 118 (1996) 731–739.
[2] J.M. Ha, G.P. Peterson, The interline heat transfer of evaporating thin films along a micro grooved surface, ASME J. Heat Transfer 118 (1996) 747–755.
[3] Jinliang Wang, Ivan, I. Catton, Enhanced evaporation heat transfer in triangular grooves covered with a thin fine porous layer, Appl. Therm. Eng. 21 (2001) 1721–1737.
[4] A. Sivaraman, S. De, S. Dasgupta, Experimental and theoretical study of axial dryout point for evaporation from V-shaped microgrooves, Int. J. Heat Mass Transfer 45 (2002) 1535–1543.
[5] I. Catton, G.R. Stroes, A semi-analytical model to predict the capillary limit of heated inclined triangular capillary grooves, ASME J. Heat Transfer 124 (2002) 162–168.
[6] J. Alario, R. Haslett, R. Kosson, The monogroove high performance heat pipe, in: AIAA Thermophysics Conference, 16th, Palo Alto, CA, June 23–25, 1981.
[7] A. Faghri, S. Thomas, Performance characteristics of a concentric annular heat pipe. Part I. Experimental prediction and analysis of the capillary limit, J. Heat Transfer 111 (1989) 844–850.
[8] S.W. Tchikanda, R.H. Nilson, S.K. Griffiths, Modeling of pressure and shear-driven flows in open rectangular microchannels, Int. J. Heat Mass Transfer 47 (2004) 527–538.
[9] R.H. Nilson, S.W. Tchikanda, S.K. Griffiths, M.J. Martinez, Steady evaporating flow in rectangular microchannels, Int. J. Heat Mass Transfer 49 (2006) 1603–1618.
[10] S.M. Yang, Heat Transfer, second ed., Higher Education Press, Beijing, China, 1987.
[11] P.C. Wayner Jr., Y.K. Kao, L.V. Lacroix, The interline heat-transfer coefficient of an evaporating wetting film, Int. J. Heat Mass Transfer 19 (1976) 487–492.
[12] P.C. Wayner Jr., A dimensionless number for the contact line evaporative heat sink, J. Heat Transfer 111 (3) (1989) 813–815.
[13] X. Xu, V.P. Carey, Film evaporation from a micro-grooved surface – an approximate heat transfer model and its comparison with experimental data, J. Thermophys. 4 (4) (1990) 512–520.
[14] J.A. Schonberg, P.C. Wayner Jr., Analytical solution for the integral contact line evaporative sink, J. Thermophys. 6 (1) (1992) 128–134.
[15] J.M. Ha, G.P. Peterson, The interline heat transfer of evaporating thin films along a micro grooved surface, J. Heat Transfer 118 (1996) 747–755.
[16] S.S. Panchamgam, J.L. Plawsky, P.C. Wayner Jr., Microscale heat transfer in an evaporating moving extended meniscus, Exp. Therm. Fluid Sci. 30 (8) (2006) 745–754.
[17] Z.Z. Xia, G.Z. Yang, R.Z. Wang, Experimental investigation of capillary-assisted evaporation on the outside surface of horizontal tubes, Int. J. Heat Mass Transfer 51 (2008) 4047–4054.